Original article

MOLECULAR METABOLISM

LRP1 in GABAergic neurons is a key link between obesity and memory function

Kellen Cristina da Cruz Rodrigues[1,8], Seung Chan Kim[1,8], Aaron Aykut Uner[1,8], Zhi-Shuai Hou[1,5,8], Jennie Young[1], Clara Campolim[1], Ahmet Aydogan[1,6], Brendon Chung[1], Anthony Choi[1], Won-Mo Yang[1], Woojin S. Kim[2], Vincent Prevot[3], Barbara J. Caldarone[4], Hyon Lee[1,7], Young-Bum Kim[1,*]

ABSTRACT

Objective: Low-density lipoprotein receptor-related protein-1 (LRP1) regulates energy homeostasis, blood—brain barrier integrity, and metabolic signaling in the brain. Deficiency of LRP1 in inhibitory gamma-aminobutyric acid (GABA)ergic neurons causes severe obesity in mice. However, the impact of LRP1 in inhibitory neurons on memory function and cognition in the context of obesity is poorly understood.

Methods: Mice lacking LRP1 in GABAergic neurons (Vgat-Cre; LRP1$^{loxP/loxP}$) underwent behavioral tests for locomotor activity and motor coordination, short/long-term and spatial memory, and fear learning/memory. This study evaluated the relationships between behavior and metabolic risk factors and followed the mice at 16 and 32 weeks of age.

Results: Deletion of LRP1 in GABAergic neurons caused a significant impairment in memory function in 32-week-old mice. In the spatial Y-maze test, Vgat-Cre; LRP1$^{loxP/loxP}$ mice exhibited decreased travel distance and duration in the novel arm compared with controls (LRP1$^{loxP/loxP}$ mice). In addition, GABAergic neuron-specific LRP1-deficient mice showed a diminished capacity for performing learning and memory tasks during the water T-maze test. Moreover, reduced freezing time was observed in these mice during the contextual and cued fear conditioning tests. These effects were accompanied by increased neuronal necrosis and satellitosis in the hippocampus. Importantly, the distance and duration in the novel arm, as well as the performance of the reversal water T-maze test, negatively correlated with metabolic risk parameters, including body weight, serum leptin, insulin, and apolipoprotein J. However, in 16-week-old Vgat-Cre; LRP1$^{loxP/loxP}$ mice, there were no differences in the behavioral tests or correlations between metabolic parameters and cognition.

Conclusions: Our findings demonstrate that LRP1 from GABAergic neurons is important in regulating normal learning and memory. Metabolically, obesity caused by GABAergic LRP1 deletion negatively regulates memory and cognitive function in an age-dependent manner. Thus, LRP1 in GABAergic neurons may play a crucial role in maintaining normal excitatory/inhibitory balance, impacting memory function, and reinforcing the potential importance of LRP1 in neural system integrity.

Keywords LRP1; GABAergic neuron; Obesity; Behavior; Memory; Neurodegeneration

[1]Division of Endocrinology, Diabetes, and Metabolism, Department of Medicine, Beth Israel Deaconess Medical Center, and Harvard Medical School, Boston, MA, USA [2]The University of Sydney, Brain and Mind Centre & School of Medical Sciences, Sydney, NSW, Australia [3]University of Lille, Inserm, CHU Lille, Laboratory of Development and Plasticity of the Neuroendocrine Brain, Lille Neuroscience & Cognition, Lille, France [4]Mouse Behavior Core, Department of Genetics, Harvard Medical School, Boston, MA, USA

[5] Present address: Key Laboratory of Mariculture (Ocean University of China), Ministry of Education (KLMME), Ocean University of China, Qingdao, China.
[6] Present address: Department of Pathology, Faculty of Ceyhan Veterinary Medicine, Cukurova University, Adana, Turkey.
[7] Present address: Department of Neurology, Gachon University Gil Medical Center, Incheon, Korea.
[8] Kellen Cristina da Cruz Rodrigues, Seung Chan Kim, Aaron Aykut Uner and Zhi-Shuai Hou contributed equally to this work.

*Corresponding author. Division of Endocrinology, Diabetes, and Metabolism, Beth Israel Deaconess Medical Center, 330 Brookline Avenue, Boston, MA, 02215 USA. E-mail: ykim2@bidmc.harvard.edu (Y.-B. Kim).

Abbreviations: LRP1, low-density lipoprotein receptor-related protein-1; LDL, low-density lipoprotein; Aβ, amyloid beta; HMS, Harvard Medical School; Vgat, vesicular GABA transporter; ELISA, enzyme linked immunosorbent assay; HOMA-IR, homeostatic model assessment for insulin resistance; PSEN1, presenilin-1; APP, amyloid precursor protein; TBS, tris-buffered saline; IL-1β, interleukin 1 beta; TNF, tumor necrosis factor; IL-6, interleukin 6; NOS2, nitric oxide synthase 2; TLR4, Toll Like Receptor 4; NLRP3, nucleotide-binding domain; leucine-rich—containing family, pyrin domain—containing-3; SOCS3, suppressor of cytokine signaling 3; CCL2, chemokine (C-C motif) ligand 2; CX3CL1, C-X3-C motif chemokine ligand 1; AIF-1, Allograft inflammatory factor 1; CD68, cluster of differentiation 68; CD11b, cluster of differentiation molecule 11B; H&E, hematoxylin and eosin; IHC, Immunohistochemistry; ABC, avidin—biotin—peroxidase complex; GFAP, glial fibrillary acidic protein; IBA1, ionized calcium binding adaptor molecule 1; GAD67, glutamic acid decarboxylase 67; DAB-H2O2, 3,3′-diaminobenzidine tetrahydrochloride; AF, Alexa fluor; FFA, free fatty acids; ApoJ, apolipoprotein J; CCFC, contextual and cued fear conditioning tasks; NMDARs, N-methyl-D-aspartate receptors; GABA, gamma-aminobutyric acid; PBS, phosphate-buffered saline; ANOVA, analysis of variance

Received June 16, 2023 • Revision received April 4, 2024 • Accepted April 10, 2024 • Available online 16 April 2024

https://doi.org/10.1016/j.molmet.2024.101941

1. INTRODUCTION

Emerging evidence from both human and animal studies underscores a significant association between obesity and cognitive decline, including brain atrophy, diminished white matter volume, compromised blood—brain barrier integrity, and heightened susceptibility to late-onset Alzheimer's disease [1—6]. Furthermore, chronic disruptions in glucose homeostasis, impaired insulin signaling, and metabolic dysfunctions are closely linked to cognitive impairments and the pathology of Alzheimer's disease [7—13]. These observations suggest the importance of maintaining normal body weight and proper fuel metabolism, which is crucial to reducing the risk of developing cognitive decline and neurodegenerative diseases.

We and others demonstrated that genetic disruption of low-density lipoprotein receptor-related protein 1 (LRP1) in the central nervous system or selectively in inhibitory gamma-aminobutyric acid (GABA) ergic neurons results in increased food intake, decreased energy expenditure, and metabolic changes leading to obesity [14,15]. LRP1, belonging to the low-density lipoprotein (LDL) receptor family, is a multi-ligand cell surface receptor broadly expressed in neurons [14,16]. Beyond its role in metabolism, LRP1 plays an important role in regulating neurotransmission, synaptic plasticity, and amyloid-β (Aβ) clearance [17—20]. Aberrant LRP1 expression has been implicated in the development of cognitive dysfunction and Alzheimer's disease-related dementia [21]. In particular, the downregulation of vascular LRP1 levels correlated with regional parenchymal and vascular accumulation of Aβ in the brains of Alzheimer's patients [22]. In line with this, evidence revealed that the deletion of LRP1 in endothelial cells of the brain led to a significant deficit in spatial learning and memory [23]. However, the specific impact of LRP1 within GABAergic neurons on cognitive function remains unexplored.

In the current study, we aim to investigate the impact of LRP1 in GABAergic neurons on cognitive function and memory while exploring the relationship between metabolic changes caused by obesity and behavioral outcomes. Here we show that LRP1 in GABAergic neurons is a crucial player between obesity and memory function.

2. MATERIALS AND METHODS

2.1. Animal care

All animal care and experimental procedures were conducted in accordance with the National Institute of Health's Guide for the Care and the Use of Laboratory Animals and approved by the Institutional Animal Care and Use Committee of Beth Israel Deaconess Medical Center and Harvard Medical School (HMS). Mice were allowed access to a standard chow diet [LabDiet, 5008 (5058 at HMS) Formulab diet, Irradiated], and water (reverse osmosis water) was provided *ad libitum*. They were housed at 22—24 °C with a 12-h light—dark cycle with the light cycle starting from 6:00 am to 6:00 pm (7:00 am—7:00 pm at HMS). Mice were single-housed for behavioral studies.

2.2. Generation of Vgat-Cre; LRP1$^{loxP/loxP}$ mice

Mice bearing a *loxP*-flanked LRP1 allele (LRP1$^{loxP/loxP}$) were purchased from The Jackson Lab (Stock No: 012604, Bar Harbor, ME). Mice lacking LRP1 in the vesicular GABA transporter (Vgat)-expressing neurons (Vgat-Cre; LRP1$^{loxP/loxP}$) were generated by mating LRP1$^{loxP/loxP}$ mice with Vgat-Cre mice (gift from Dr. Brad Lowell, Beth Israel Deaconess Medical Center, Boston, MA). These mice were derived from 129 ES cells in C57BL/6 embryos. All mice studied had a mixed background with 129 and C57BL/6. LRP1 expression was reduced in the arcuate nucleus, paraventricular hypothalamic nucleus, and dorsomedial hypothalamic nucleus of Vgat-Cre; LRP1$^{loxP/loxP}$ mice where Vgat is expressed [14]. Vgat-Cre; LRP1$^{loxP/loxP}$ and LRP1$^{loxP/loxP}$ littermates were used for analyses. Healthy mice showing normal behavior, development, and constant physical activity (although obese) were used. Mice were excluded from the experiments if they showed abnormal development, such as hydrocephalus.

2.3. Measurements of Aβ and metabolic parameters

Mice were weighed from 4 weeks of birth and weekly thereafter. Epididymal fat was harvested and weighed at the end of the experiment in male mice at 32 weeks of age. Blood was collected from overnight fasted mice via the tail. Blood glucose was measured using a OneTouch Ultra glucose meter (LifeScan, Inc., Milpitas, CA). Serum levels of insulin (90080, Crystal Chem, Chicago, IL), leptin (90030, Crystal Chem, Chicago, IL), apolipoprotein J (ApoJ) (MCLU00, R&D Systems, Minneapolis, MN), $A\beta_{40}$ (KMB3481, Thermo Fisher Scientific Inc., Waltham, MA), $A\beta_{42}$ (KMB3441, Thermo Fisher Scientific Inc., Waltham, MA) and free fatty acids (FFA) (ab65341, Abcam, Waltham, MA) were measured by enzyme-linked immunosorbent assay (ELISA). The homeostatic model assessment for insulin resistance (HOMA-IR) was calculated as [fasting glucose (mmol/L) × fasting insulin (μIU/mL)]/22.5 with a slight modification in insulin conversion as has recently been recommended [24,25].

2.4. Immunoblotting analysis

Tissue lysates were resolved by sodium dodecyl sulfate—polyacrylamide gel electrophoresis and transferred to nitrocellulose membranes (GE Healthcare Life Sciences, Pittsburgh, PA). The membranes were incubated with polyclonal antibodies against presenilin-1 (PSEN1) (sc-365450, Santa Cruz Biotechnology Inc., Dallas, TX), amyloid precursor protein (APP) (A8717, Sigma—Aldrich, St. Louis, MO), cleaved caspase 3 (9661, Cell Signaling Technology, Danvers, MA) or monoclonal antibody against β-actin (A2228, Sigma—Aldrich, St. Louis, MO). The membranes were washed with Tris-buffered saline (TBS) containing 0.1% Tween 20 for 30 min, incubated with horseradish peroxidase secondary antibodies against mouse (7076, Cell Signaling Technology, Danvers, MA) or rabbit (7074, Cell Signaling Technology) for 1 h, and washed with TBS containing 0.1% Tween 20 for 30 min. The bands were visualized with enhanced chemiluminescence and quantified by an ImageJ program (v1.52a, NIH). All protein levels were normalized by β-actin levels.

2.5. RNA isolation and mRNA measurement

Total RNA was isolated by the Trizol Reagent (Invitrogen, CA). Single-strand cDNA was synthesized from total RNA using a reverse transcription (RT-PCR) kit (Applied Biosystems, Woburn, MA) according to the manufacturer's instructions. The PCR reactions were performed in a 20 μl volume containing 15 ng of cDNA for 40 cycles. The sequence of the primers used for qPCR is listed in Supplementary Table 1. The relative content of mRNAs was determined after normalization with GAPDH using the ΔΔCT method.

2.6. Locomotor activity

Mice were placed in the center of a square Plexiglas box (27 cm × 27 cm × 20.3 cm) containing infrared arrays (Med Associates, St Albans, VT, USA) and allowed to explore the environment for 1 h freely. The total activity (cm) was recorded using specialized software (Activity Monitor, Version 5.9).

2.7. Spatial Novelty Y Maze

The Spatial Novelty Y Maze is a two-trial short-term memory test measuring a mouse's preference for exploring a novel environment. In the first forced trial, the mouse is placed in the "start" arm and is allowed to explore both the "start" and "familiar" arm. After a short delay, the mouse is given a free choice to explore the "familiar" or "novel" arm. If the mouse remembers the familiar arm, it should choose to explore the "novel" more than the "familiar" arm. Testing was conducted in a clear acrylic Y maze with three arms (one start arm and two test arms, all ~31 cm long). The testing room had distinct visual cues, and the maze had a removable partition to block the appropriate arm. The blocked arm was randomized and balanced for each genotype. The test consisted of a forced-choice trial followed by a free-choice trial. For the forced choice trial, the start arm and one test arm were open, with access to the second test arm blocked by the partition. Individual subjects were placed in the start arm and allowed to explore the open test arm for 3 min, after which they were removed from the maze, and placed in a holding cage as the maze was cleaned. The partition was removed and the mice were then placed back into the Y maze for the free choice trial and allowed to explore both the open and test arms for 3 min. The delay between the forced choice and free choice trials was 2 min. Animal behavior was video recorded during both trials, and the time spent in the previously accessible arm (i.e., familiar arm) and the previously blocked arm (i.e., novel arm) was determined during the free choice trial using Ethovision software. For each subject, the % time and distance exploring the novel arm during the free choice trial is calculated using the formula: % novel = novel/(novel + familiar) x 100.

2.8. Rotarod test

Motor coordination was assessed using a rotarod test (Ugo Basile, Gemonio, VA, Italy). Mice were first given a 5 min habituation trial in which the mice were placed on the apparatus that was rotating at a constant speed of 4 rpm. If mice fell off during this acclimation period, they were placed back on the rod. Mice were then given two test trials, in which the rod accelerated at 4–40 rpm over a course of 3 min. The maximum cutoff time was 5 min. When mice fell off the rod, the latency to fall was recorded. Mice were given a 3 h interval between trials. The average of the two trials was calculated.

2.9. Water T-maze

A custom-made Plexiglas plus maze testing apparatus (each arm 36 cm length, 10 cm width, 21 cm height) (Plastic Craft, West Nyack, NY) with four arms (North, South, East, and West) was used to evaluate spatial memory. One arm was blocked off with a divider so the mouse could choose one of the east and west arms to escape. An escape platform was placed on the east side of the maze ~1 cm below the surface water. The maze was filled with 23–26 °C water and white non-toxic paint to ensure the mouse could not see the escape platform. After a 10 min acclimation period in the testing room, the mouse was placed into the appropriate arm facing the wall and was allowed to swim until it found the escape platform. The start position was alternated (north and south) in a semi-randomized order. If the mouse was not able to find the escape platform within 1 min, the experimenter guided the mouse to the platform. The mouse was allowed to stay on the platform for 10 s before being placed back into its holding cage. Mice were tested for 5 days (10 trials/day), and correct and incorrect choices to find the escape platform were recorded. Once both control and knockout mice reached the acquisition criteria, which was a group mean of 80% or more correct responses, the escape platform was moved to the opposite side (west), and reversal learning was conducted for 5 days.

2.10. Contextual and cued fear conditioning tasks (CCFC)

Mice were placed in Plexiglas conditioning chambers (Med Associates, St. Albans, VT) with speakers (Med Associates Sound generator ENV-230, St. Albans, VT) and steel bars spaced 1 cm apart for electric shocks (0.5 mA). On the first day (training phase), after a 2 min acclimation period, the mice received two tones (30 s) and electric shocks (2 s) within the last 2 s of the tone with a 2 min inter-trial interval. On day 2, the mice were placed in the chamber but did not receive a tone and electric shock. Freezing behavior was recorded for 5 min in the conditioning context and analyzed by the Ethovision Software (EthoVision XT 14, Noldus, Wageningen, the Netherlands). After all mice were tested for contextual fear conditioning, the context was changed by inserting a white Plexiglas floor over the shock grid and white Plexiglas to cover the wall. Freezing was measured for 3 min in this altered context and for 3 min during the presentation of the tone. Two weeks after the last behavior test, mice were sacrificed, and brain tissues were harvested for further analysis.

2.11. Histopathology

Mice were transcardially perfused with phosphate-buffered saline (PBS) followed by a 10% formalin solution. Brains were removed, cut sagittally at the center, and left hemispheres were fixed overnight in 10% neutral formalin solution. They were then processed using graded alcohols and xylene, embedded in paraffin, sectioned at 5 μm (lateral from ~0.18 mm to 1.5 mm), stained with hematoxylin and eosin (H&E) (MHS32, Sigma–Aldrich, Louis, MO), and images of the whole hippocampal sections were acquired on a light microscope (Zeiss AxioImager M1, Göttingen, Germany) [26]. Necrotic neurons with perineural satellitosis, as well as microglial cells in the hippocampus, were counted from the acquired images on ImageJ software (National Institutes of Health, USA).

2.12. Immunohistochemical staining

Immunohistochemistry (IHC) was performed on 5-μm paraffin sections using the standard avidin–biotin–peroxidase complex (ABC) method according to the manufacturer's recommendations (Mouse and Rabbit Specific HRP/DAB (ABC) Detection IHC kit (ab64264), Abcam, Waltham, MA). Sections were subjected to routine deparaffinization in xylene and then rehydration in ethanol (100%, 80%, and 50%). Inhibition of endogenous peroxidase activity and blocking of non-specific binding were performed according to the kit's instructions. Antigen retrieval for all markers was done by microwaving the sections in citrate buffer (pH = 6.0) at a sub-boiling temperature for 5 min. After a protein blocking, brain sections were incubated with primary antibodies overnight at 4 °C. The primary antibodies used were anti-glial fibrillary acidic protein (GFAP) antibody (dilution; 1:100, Sigma–Aldrich (G6171), St. Louis, MO), anti-ionized calcium binding adaptor molecule 1 (IBA1) antibody (dilution; 1:100, Wako (019–19741), Richmond, VA), anti-glutamic acid decarboxylase 67 (GAD67) antibody (clone 1G10.2, dilution; 1:100, Sigma–Aldrich (MAB5406)) and anti-N-methyl-D-aspartate receptor 1 (NMDAR1) antibody (dilution; 1:50, Invitrogen (32-0500)). The brown color of immunopositivity in brain sections was developed with 3,3′-diaminobenzidine tetrahydrochloride (DAB-H2O2) substrate for 10 min. Slides were counterstained with Mayer's hematoxylin (Sigma–Aldrich), dehydrated, and mounted with Entellan (Sigma–Aldrich). On each slide, immunopositive reactions were detected by the presence of brown cytoplasmic staining.

Immunopositive cells of GAD67 were counted as described in the histopathology section (2. 11.), and other markers were counted with the computed assistance of the Analyze Particles plugin on ImageJ, utilizing color-thresholded binary images.

2.13. Double immunofluorescent staining

Double immunofluorescent staining was performed to confirm the knockdown of LRP1 from GABAergic neurons. Mice were transcardially perfused as described in the histopathology section. Brains were removed, cut sagittally at the center, and right hemispheres were incubated in 10% formalin and then 30% sucrose solution (overnight each). They were washed with PBS, embedded in Tissue Tek OCT (Sakura Finetek), and frozen at −80 °C. Frozen brain tissues were cryo-sectioned at 16 μm (lateral from ∼0.24 mm to 2.04 mm) and transferred on Superfrost Plus microscope slides (Thermo Fisher Scientific). Sections were washed with PBS, permeabilized in 0.25% Triton X-100 (15 min at room temperature), blocked in 10% normal donkey serum (1 h at room temperature), and then incubated overnight in blocking solution containing primary antibody [Lrp1 (rabbit) dilution; 1:500, Abcam (ab92544); Lrp1 (mouse) dilution; 1:100, Invitrogen (37-3800); GAD67 (clone 1G10.2) dilution; 1:200, Sigma—Aldrich (MAB5406)] at room temperature. The next day, the sections were washed and then incubated in secondary antibodies [Alexa fluor (AF) 488 and AF 647 dilution; 1:500]. After washing, the sections were mounted with UltraCruz® Hard-set Mounting Medium with DAPI (Santa Cruz), and images of double immunofluorescent positive cells (LRP1 vs GAD67) in the hippocampus were acquired with a confocal microscope (Zeiss LSM 880).

2.14. Statistical analysis

A power analysis was conducted using G Power (Version 3.1.9.2, Germany) to estimate the sample size. The probability of α and β errors was set at 0.05 and 0.20, respectively. The effect size was calculated according to the software's instructions or preliminary data, if any. The data were checked for the normality of distribution by the Shapiro—Wilk test. Logarithmic transformation or non-parametric tests were done if the data were not distributed normally. The student t-test or Mann—Whitney U test was conducted to compare two groups. The paired t-test or Wilcoxon test was used when comparing the data within groups. Two-way analysis of variance (ANOVA) was done when two independent factors [e.g. time-group or arm (familiar/novel)-group] might have an effect. *Post hoc* multiple comparisons were carried out using the Sidak test in GraphPad Prism (GraphPad Prism, Version 8.0.1, La Jolla, CA) or general linear procedures in SPSS (extra coding was applied on the syntax menu) (SPSS 26.0 software for Windows; SPSS Inc., Chicago, IL). Body weight was used as a covariate when appropriate. Correlations were done using Pearson's or Spearman correlation analyses depending on the data distribution. $P \leq 0.05$ was considered significant. The results were presented as mean ± standard error of the mean (SEM).

3. RESULTS

3.1. Deletion of LRP1 in GABAergic neurons causes severe obesity

The deletion of LRP1 in GABAergic neurons significantly decreased the LRP1 levels in cortex (Supplementary Figure 1A), hippocampus (Supplementary Figure 1C), spinal cord with pons (Supplementary Figure 1E), and olfactory bulb (Supplementary Figure 1F) in Vgat-Cre; $LRP1^{loxP/loxP}$ compared to $LRP1^{loxP/loxP}$ mice, and tended ($p = 0.0577$) to decrease in cerebellum (Supplementary Figure 1D). However, the expression of LRP1 was normal in the hypothalamus (Supplementary Figure 1B). Consistent with the reduction of LRP1 in the hippocampus, double immunofluorescent staining of GABAergic neuronal marker GAD67 and LRP1 showed colocalization only in $LRP1^{loxP/loxP}$ mice (Supplementary Figure 1H), while Vgat-Cre; $LRP1^{loxP/loxP}$ mice did not show any colocalization of GAD67 and LRP1 (Supplementary Figure 1H), confirming LRP1 deletion in GABAergic neurons. Consistent with our previous findings [14], we observed that mice lacking LRP1 in GABAergic neurons were severely obese (Figure 1A) with increases in epididymal fat (Figure 1B). Serum levels of leptin (Figure 1C) and insulin (Figure 1G) were also increased in Vgat-Cre; $LRP1^{loxP/loxP}$ mice compared with $LRP1^{loxP/loxP}$ mice at 32 weeks of age. However, neither serum FFA nor blood glucose levels were altered in Vgat-Cre; $LRP1^{loxP/loxP}$ mice (Figure 1D,F). Vgat-Cre; $LRP1^{loxP/loxP}$ mice were insulin resistant, as demonstrated by increased HOMA-IR index (Figure 1H). In addition, we found that Vgat-Cre; $LRP1^{loxP/loxP}$ mice at 16 weeks of age had elevated body weight (Figure 1I). However, neither the blood glucose (Figure 1J), serum insulin (Figure 1K), or serum leptin levels (Figure 1L) were not altered in Vgat-Cre; $LRP1^{loxP/loxP}$ mice compared with $LRP1^{loxP/loxP}$ mice. These results suggest that LRP1 action in GABAergic neurons is required to regulate body weight and metabolic homeostasis. These effects are likely due to increased food intake and energy imbalance [14].

3.2. Mice lacking LRP1 in GABAergic neurons have increased serum ApoJ levels

ApoJ has been implicated in the pathogenesis of Alzheimer's disease [27—30]. Given that LRP1 is a potential receptor for ApoJ [31,32] and serum ApoJ levels are elevated in humans with obesity and type 2 diabetes as well as diet-induced obese mice [33—35], we measured ApoJ levels in the serum and tissues of Vgat-Cre; $LRP1^{loxP/loxP}$ mice. We found that serum ApoJ levels significantly elevated in Vgat-Cre; $LRP1^{loxP/loxP}$ mice at 32 weeks (Figure 1E) and at 16 weeks (Figure 1M) of age compared to $LRP1^{loxP/loxP}$ mice, whereas ApoJ levels in the liver, brain, hippocampus, and cerebral cortex remained unaltered (Supplementary Figure 2A—D). Furthermore, there was a strong correlation between serum ApoJ levels at 32 weeks of age and body weight, serum insulin, and leptin levels (Supplementary Figure 2F-H). These findings suggest increased serum ApoJ levels are associated with LRP1-mediated metabolic dysfunction.

3.3. LRP1 in GABAergic neurons regulates motor function and spatial recognition memory

Locomotor activity and rotarod tests were assessed to determine whether GABAergic deletion of LRP1 alters motor activity and coordination. Vgat-Cre; $LRP1^{loxP/loxP}$ mice displayed a significant decrease in the total distance traveled over 1 h (Figure 2A) and in 5 min intervals (Figure 2B) compared with $LRP1^{loxP/loxP}$ mice. These effects were associated with reduced rotarod performance in Vgat-Cre; $LRP1^{loxP/loxP}$ mice (Figure 2C). When the body weights of mice were used as covariates, we found that the total distance (Figure 2A) and the distance traveled in 5 min intervals (Figure 2B) were no longer significantly different between groups while the values of motor coordination remained significant (Figure 2C). Mice were subjected to the Y-maze test to determine whether LRP1 activity in GABAergic neurons is involved in short-term memory. The distance traveled and time spent in the familiar arm were similar between $LRP1^{loxP/loxP}$ and Vgat-Cre; $LRP1^{loxP/loxP}$ mice (left panels of Figure 2D,F), and the distance traveled and time spent in the novel arm was increased compared with the familiar arm for both groups (right panels of Figure 2D,F), indicating that both groups are capable of learning and memory. However, mice lacking LRP1 in GABAergic neurons visited the novel arm less frequently

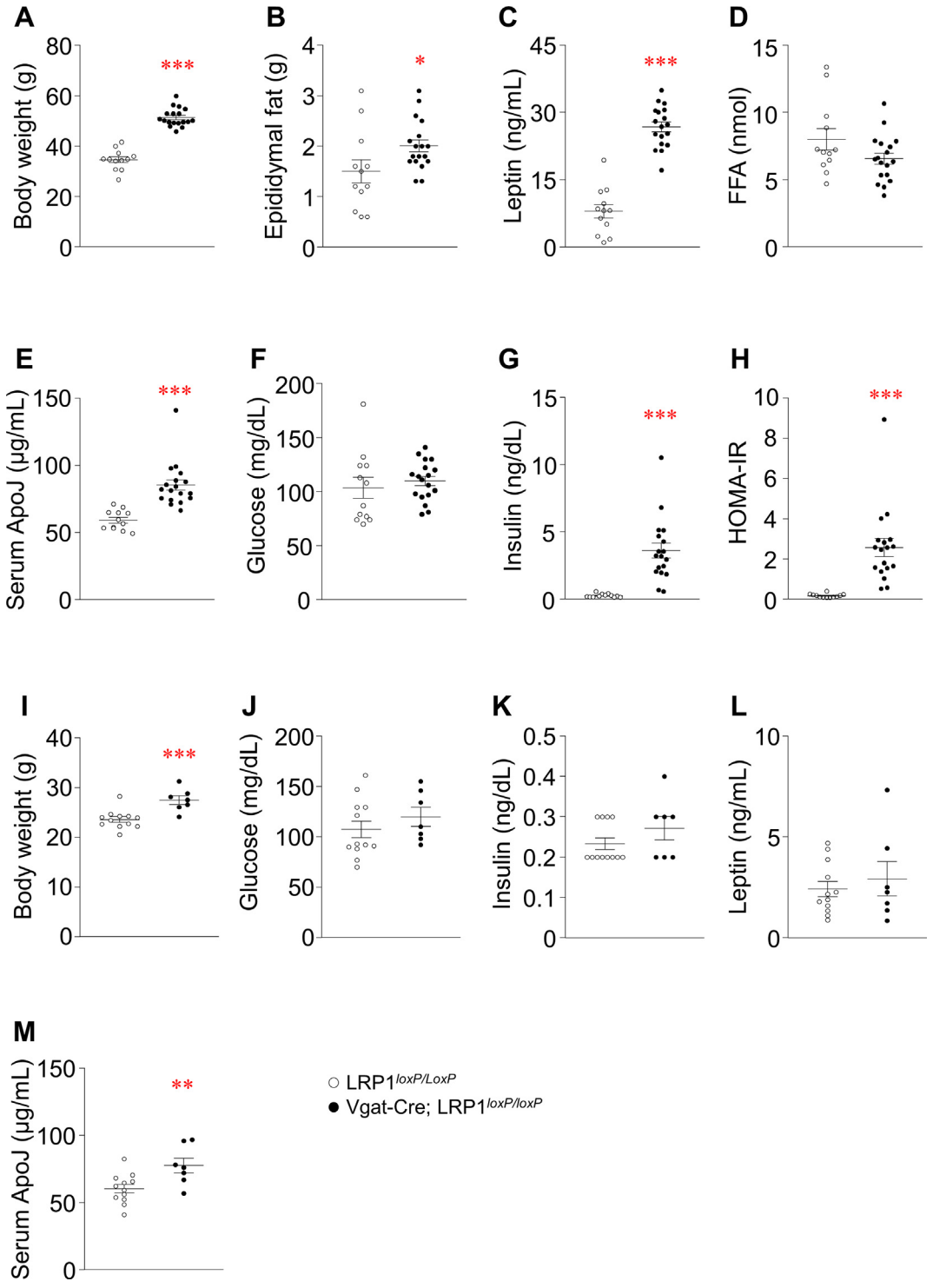

Figure 1: Selective deletion of LRP1 in GABAergic neurons causes metabolic disorders. (**A**) Body weight, (**B**) epididymal fat, (**C**) serum leptin, (**D**) serum FFA, (**E**) serum ApoJ, (**F**) blood glucose, (**G**) serum insulin, and (**H**) HOMA-IR were measured in LRP1$^{loxP/loxP}$ and Vgat-Cre; LRP1$^{loxP/loxP}$ male mice that were overnight fasted mice at 32 weeks of age. $n = 12$ for control, $n = 18$ for Vgat-Cre; LRP1$^{loxP/loxP}$. (**I**) Body weight, (**J**) blood glucose, (**K**) serum insulin, (**L**) serum leptin, and (**M**) serum ApoJ were measured in LRP1$^{loxP/loxP}$ and Vgat-Cre; LRP1$^{loxP/loxP}$ male mice that were overnight fasted at 16 weeks of age. $n = 12$ for control, $n = 7$ for Vgat-Cre; LRP1$^{loxP/loxP}$. All graphs represent means or individual values ± SEM. $^{*}P < 0.05$, $^{**}P < 0.01$, $^{***}P < 0.001$ vs. LRP1$^{loxP/loxP}$ by two-sided Student's t-test.

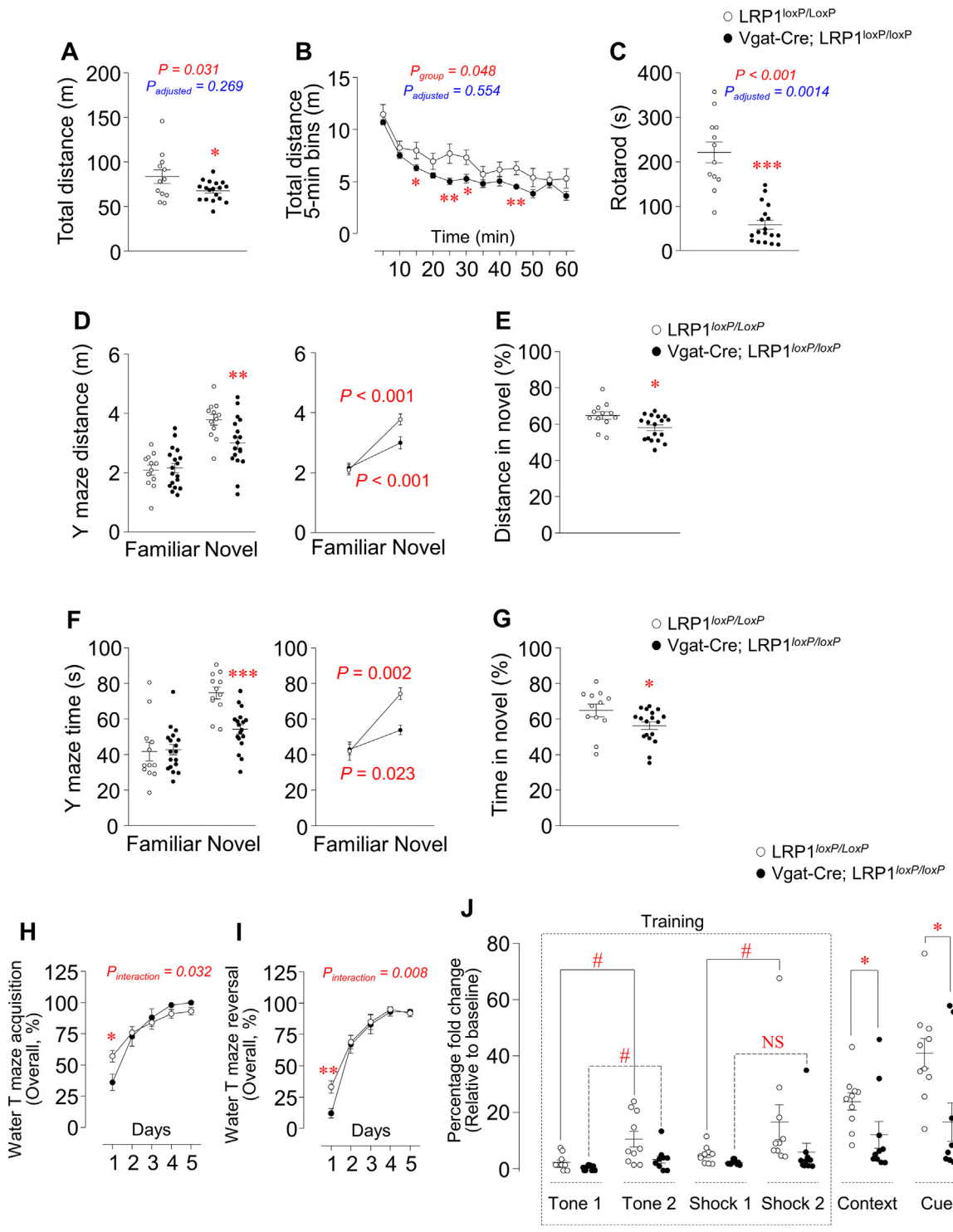

Figure 2: Effect of LRP1 deletion in GABAergic neurons on motor coordination, learning, and memory. (**A**) Total distance traveled in 1 h on the locomotion test, (**B**) distance traveled in 5 min intervals on the locomotion test, (**C**) latency to fall on the rotarod test, (**D**) total distance traveled in novel and familiar arms on the spatial Y-maze test (left panel), and changes in total distance traveled from the familiar to novel arm (right panel), (**E**) percentage of distance traveled in the novel arm of spatial Y-maze, (**F**) time spent in the novel and familiar arms on the spatial Y-maze test (left panel), and changes in time spent from the familiar to novel arm (right panel), and (**G**) percentage of time spent in the novel arm of the spatial Y-maze in LRP1$^{loxP/loxP}$ and Vgat-Cre; LRP1$^{loxP/loxP}$ male mice. $n = 12$ for control, $n = 18$ for LRP1$^{loxP/loxP}$ (26 weeks old). All graphs represent means or individual values ± SEM. $^{*}P < 0.05$, $^{**}P < 0.01$, $^{***}P < 0.001$ vs. *LRP1$^{loxP/loxP}$* by two-sided Student's t-test. D and F data in the right panels were evaluated by paired t-test. The adjusted *P* values in A, B, and C were calculated by the covariance analysis (body weight was used as a covariate). Percentage correct response (10 trials/day) of LRP1$^{loxP/loxP}$ ($n = 10$) and Vgat-Cre; LRP1$^{loxP/loxP}$ ($n = 10$) male mice (28–29 weeks old) on the (**H**) acquisition and (**I**) reversal water T-maze. $^{*}P < 0.05$, $^{**}P < 0.01$ by two-way ANOVA (*post hoc* tests were done using GLM procedures on SPSS). (**J**) Percentage fold change (relative to baseline) in freezing time of LRP1$^{loxP/loxP}$ ($n = 10$) and Vgat-Cre; LRP1$^{loxP/loxP}$ ($n = 10$) male mice (31 weeks old) during the fear conditioning test. $^{\#}P < 0.05$ by paired t-test or Wilcoxon test.

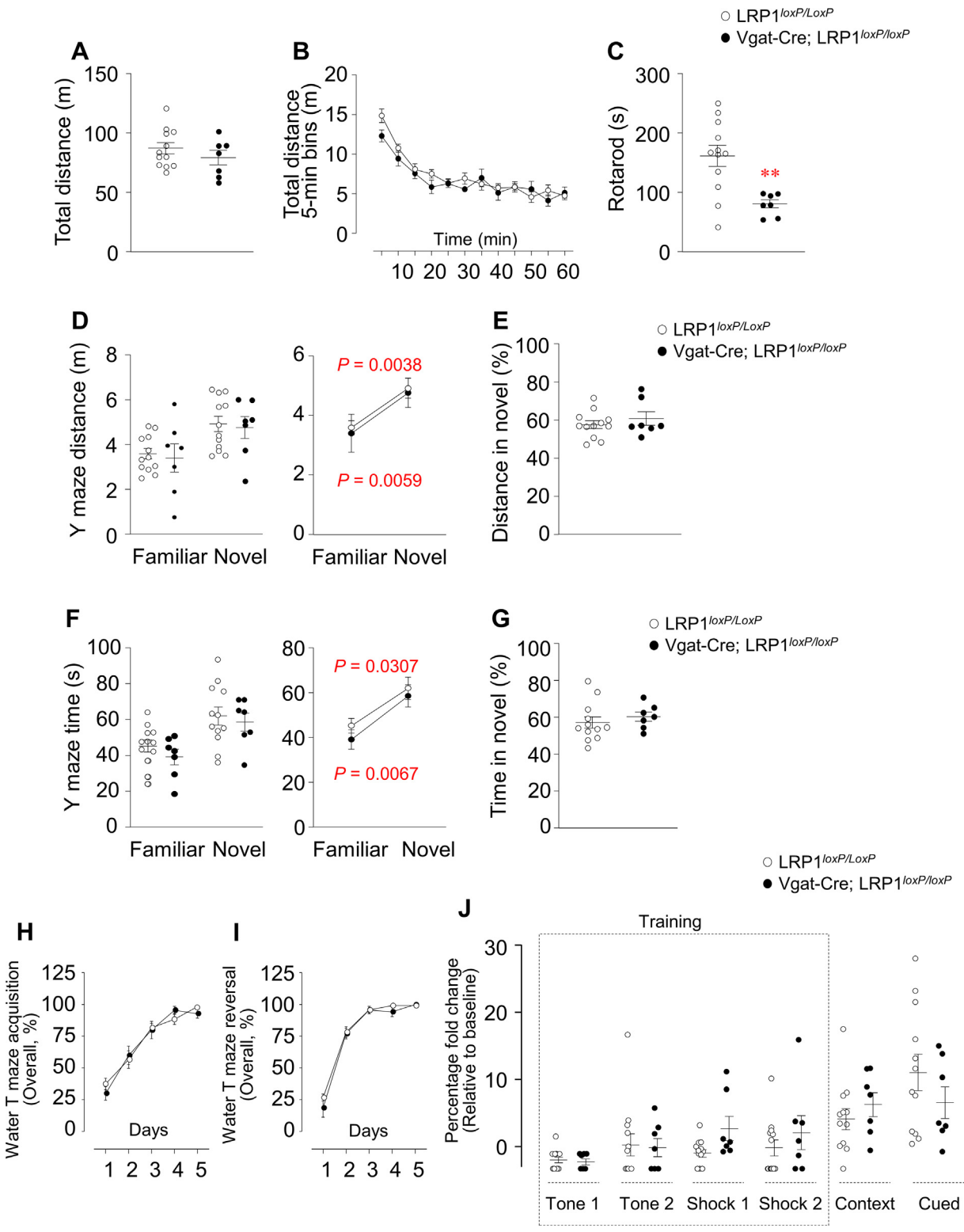

Figure 3: Effect of LRP1 deletion in GABAergic neurons on motor coordination, learning, and memory in 16-week-old mice. (**A**) Total distance traveled in 1 h on the locomotion test, (**B**) distance traveled in 5 min intervals on the locomotion test, (**C**) latency to fall on the rotarod test, (**D**) total distance traveled in novel and familiar arms on the spatial Y-maze test (left panel), and changes in total distance traveled from the familiar to novel arm (right panel), (**E**) percentage of distance traveled in the novel arm of spatial Y-maze, (**F**) time spent in the novel and familiar arms on the spatial Y-maze test (left panel), and changes in time spent from the familiar to novel arm (right panel), and (**G**) percentage of time spent in the novel arm of the spatial Y-maze in LRP1$^{loxP/loxP}$ and Vgat-Cre; LRP1$^{loxP/loxP}$ male mice. $n = 12$ for control, $n = 7$ for LRP1$^{loxP/loxP}$ (10 weeks old). D and F data in the right panels were evaluated by paired t-test. All graphs represent means or individual values ± SEM. $^{**}P < 0.01$ vs. LRP1$^{loxP/loxP}$ by two-sided Student's t-test. Percentage correct response (10 trials/day) of LRP1$^{loxP/loxP}$ ($n = 12$) and Vgat-Cre; LRP1$^{loxP/loxP}$ ($n = 7$) male mice (12–14 weeks old) on the (**H**) acquisition and (**I**) reversal water T-maze. (**J**) Percentage fold change (relative to baseline) in freezing time of LRP1$^{loxP/loxP}$ ($n = 12$) and Vgat-Cre; LRP1$^{loxP/loxP}$ ($n = 7$) male mice (15 weeks old) during the fear conditioning test.

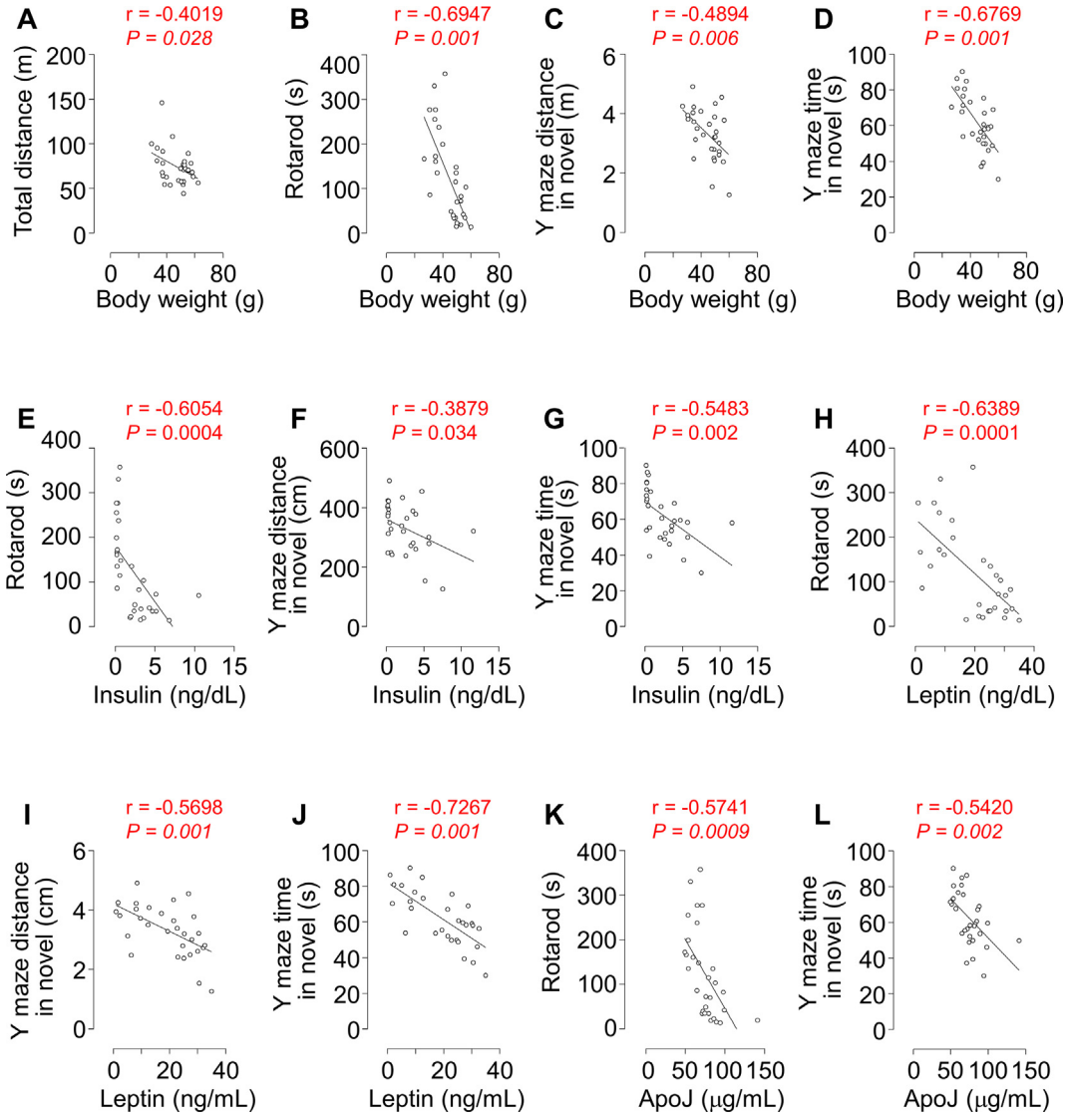

Figure 4: Relationship of motor function, motor coordination, and spatial recognition memory with obesity-linked metabolic parameters. Correlation of body weight with (**A**) total distance traveled on the locomotion test, (**B**) latency to fall on the rotarod test, (**C**) total distance traveled, and (**D**) time spent in the novel arm on the spatial Y-maze test was evaluated. Correlation of serum insulin with (**E**) latency to fall on the rotarod test, (**F**) total distance traveled, and (**G**) time spent in the novel arm on the spatial Y-maze test was evaluated. Correlation of serum leptin with (**H**) latency to fall on the rotarod test, (**I**) total distance traveled, and (**J**) time spent in the novel arm on the spatial Y-maze test was evaluated. Correlation of serum ApoJ with (**K**) latency to fall on the rotarod test and (L) time spent in the novel arm on the spatial Y-maze test were evaluated. The *P* values were obtained by Pearson correlation analysis, and the r values indicate Pearson correlation coefficient. All correlations were analyzed from the data of LRP1$^{loxP/loxP}$ and Vgat-Cre; LRP1$^{loxP/loxP}$ male mice (32 weeks old).

(Figure 2D left panel and E) and spent less time there (Figure 2F left panel and G) than LRP1$^{loxP/loxP}$ mice. On the other hand, when we performed locomotor activity (Figure 3A—B) and Y-maze (Figure 3D—G) tests in 10—11-week-old mice, we did not observe impairment in motor activity and short-term memory in Vgat-Cre; LRP1$^{loxP/loxP}$ mice. Motor coordination seems to be the first ability to be affected by the deletion of LRP1 in GABAergic neurons since the rotarod (Figure 3C) test was altered in Vgat-Cre; LRP1$^{loxP/loxP}$ mice. These observations demonstrate that LRP1 in GABAergic neurons may play a role in regulating motor function and spatial short-term memory in an age-dependent manner.

3.4. LRP1 in GABAergic neurons is involved in cognition and learning

We tested mice in the water T-maze and CCFC to further determine the impact of LRP1 activity on cognition and learning memory. In the water T-maze test, the average percentage of correct responses to find the hidden escape platform on the first day of the acquisition was lower in Vgat-Cre; LRP1$^{loxP/loxP}$ mice compared to controls, but no differences were observed on day 2—5 (Figure 2H). Similar results were found when the escape platform was placed on the opposite side (reversal) (Figure 2I).

In the CCFC test, *Vgat-Cre; LRP1$^{loxP/loxP}$* mice displayed a higher baseline freezing time on the training day than LRP1$^{loxP/loxP}$ mice. We therefore adjusted the results [including the training day (Figure 2J)] according to the baseline values of the training day. The adjusted data revealed that on the training day, all mice increased their freezing time slightly or significantly on tone 2 and shock 2 compared to tone 1 and shock 1 (Figure 2J), indicating a recognition of the neutral (tone) and aversive (shock) stimuli. However, Vgat-Cre; LRP1$^{loxP/loxP}$ mice exhibited less freezing time compared to the control mice on the second day in CCFC tests (Figure 2J). We observed normal cognition and learning function in Vgat-Cre; LRP1$^{loxP/loxP}$ mice aged 12–15 weeks when we conducted tests on T-maze (Figure 3H–I) and CCFC (Figure 3J). Together, these findings suggest age-dependent effects of LRP1 action on cognition and learning.

3.5. Perturbed metabolic profiles are associated with cognitive dysfunction in mice lacking GABAergic

We performed correlation analyses between behavioral and metabolic parameters to determine the relationship between cognitive function and metabolic profiles. Total travel distance is negatively correlated with body weight (Figure 4A). Motor coordination is negatively correlated with body weight (Figure 4B), serum insulin (Figure 4E), serum leptin (Figure 4H), and serum ApoJ (Figure 4K) levels. Total travel distance and duration in the novel arm, as measured by the Y-maze test, negatively correlated with metabolic parameters, including body weight (Figure 4C–D), serum insulin (Figure 4F–G), leptin (Figure 4I–J), and ApoJ (Figure 4L).

Similar to the Y-maze correlation results, body weight (Figure 5A) and the serum levels of leptin (Figure 5B), insulin (Figure 5C), and ApoJ (Figure 5D) negatively correlated with the data from the reversal water T-maze test. Body weight (Figure 5E), serum leptin (Figure 5F), and insulin (Figure 5G) did not correlate with the water T-maze acquisition, but serum ApoJ levels (Figure 5H) negatively correlated with it.

In 16-week-old mice, we did not observe the association between metabolic profiles and most cognitive function tests (Supplementary Figure 3A, B-J, L, and Supplementary Figure 4A-H). However, a negative correlation between motor coordination and serum ApoJ was detected (Supplementary Figure 3K). These results suggest that there may be a potential link between obesity and dysregulated locomotor activity, motor coordination, or spatial recognition memory in 32-week-old mice.

3.6. The effect of LRP1 deficiency on Aβ level

Since LRP1 plays an important role in Aβ clearance [19], we measured Aβ levels in the serum, brain, and liver to understand the impact of GABAergic neuron-specific LRP1 deficiency on Aβ production. The levels of $A\beta_{42}$ trended higher in the serum and brain of Vgat-Cre; LRP1$^{loxP/loxP}$ mice but not in the liver compared with LRP1$^{loxP/loxP}$ mice (Supplementary Figure 5A–C). Serum and brain $A\beta_{40}$ levels tended to be decreased, while hepatic levels were significantly elevated in Vgat-Cre; LRP1$^{loxP/loxP}$ mice (Supplementary Figure 5D–F). The ratio of $A\beta_{42/40}$ was significantly higher in Vgat-Cre; LRP1$^{loxP/loxP}$ mice than LRP1$^{loxP/loxP}$ mice (Supplementary Figure 5G). Deletion of LRP1 in GABAergic neurons tended to decrease hippocampal PSEN1 levels, while it did not affect PSEN1 levels in cortex and hippocampal APP levels (Supplementary Figure 5H–I).

3.7. Deficiency of LRP1 in GABAergic neurons causes neurodegeneration

We performed a histopathological evaluation of the hippocampus to determine whether the loss of LRP1 in GABAergic neurons leads to neurodegeneration in an age-dependent manner in either 16-week mice (Figure 6A) or 32-week mice (Figure 6B). We examined both LRP1$^{loxP/loxP}$ and Vgat-Cre; LRP1$^{loxP/loxP}$ mice and found that they showed some degree of necrotic change in the hippocampus, such as neuronal shrinkage, darker cytoplasm, and pyknosis. These changes greatly increased in the hippocampus of the 32-week Vgat-Cre;

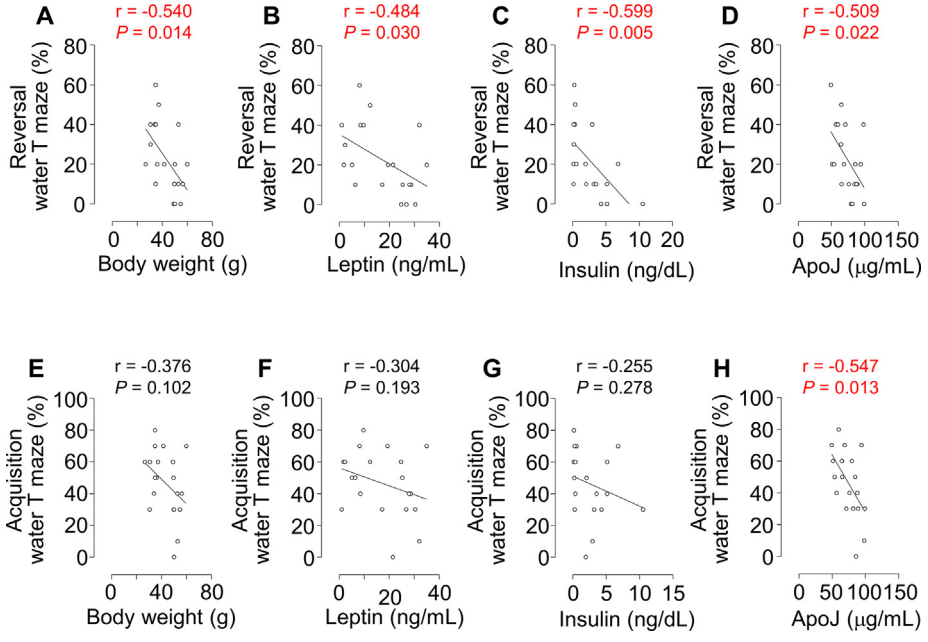

Figure 5: Relationship between metabolic parameters and cognitive function. Correlation of body weight, serum leptin, serum insulin, and serum ApoJ with the data from acquisition (**A, C, E, G**) and reversal (**B, D, F, H**) water T-maze on day 1 was evaluated. The *P* values were obtained by Pearson correlation analysis and r values indicate the Pearson correlation coefficient. All correlations were analyzed from the data of LRP1$^{loxP/loxP}$ and Vgat-Cre; LRP1$^{loxP/loxP}$ male mice (32 weeks old).

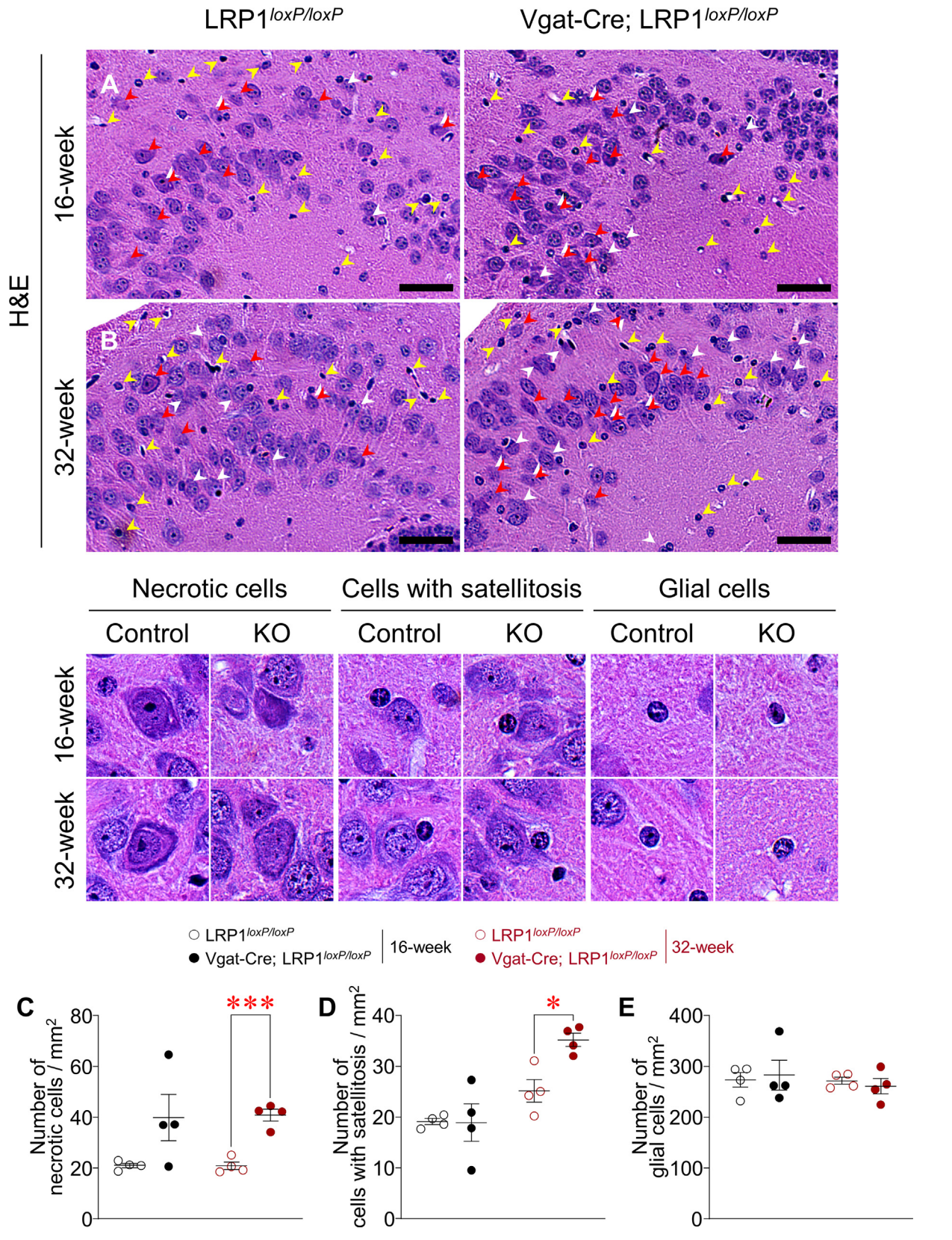

Figure 6: Histopathological features in the hippocampus of GABAergic neuron-specific LRP1-deficient mice at different ages. H&E staining of (**A**) 16-week LRP1$^{loxP/loxP}$ and Vgat-Cre; LRP1$^{loxP/loxP}$ male mice (16 weeks old, n = 4 per group), and (**B**) 32-week LRP1$^{loxP/loxP}$ and Vgat-Cre; LRP1$^{loxP/loxP}$ male mice (32 weeks old, $n = 4$ per group). White arrows indicate necrotic changes in neurons, red arrows indicate neurons with satellitosis, and yellow arrows indicate glial cells in the hippocampus. (**C**) Necrotic neurons, (**D**) perineural satellitosis, and (**E**) glial cells in the hippocampus from 16-week and 32-week-old mice were counted. Scale bars represent 50 μm. All graphs represent means or individual values ± SEM. $^{*}P < 0.05$, $^{***}P < 0.001$ vs. LRP1$^{loxP/loxP}$ by two-sided Student's t-test, H&E: Hematoxylin and eosin.

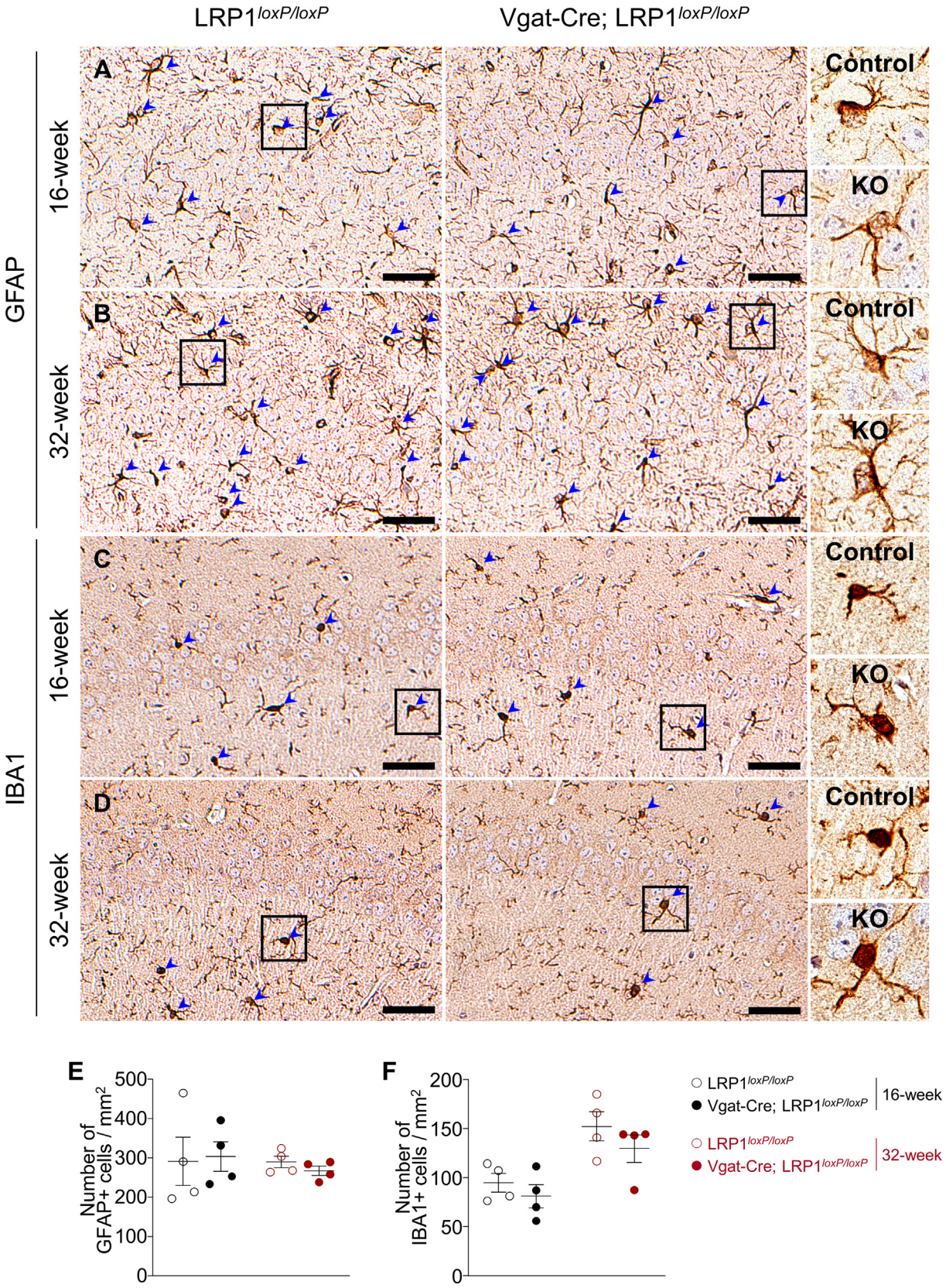

Figure 7: Immunohistochemical analysis of GFAP and IBA1 in the hippocampus of GABAergic neuron-specific LRP1-deficient mice at different ages. (**A, B**) GFAP, and (**C, D**) IBA1 immunoreactivity of LRP1$^{loxP/loxP}$ and Vgat-Cre; LRP1$^{loxP/loxP}$ mice at different ages (16 and 32 weeks old, n = 4 per group). Arrows indicate GFAP^{+} and IBA1^{+} cells in the hippocampus. These cells were counted. Graphs represent the quantitation of GFAP^{+} and IBA1^{+} cells in the whole hippocampal areas, which were normalized to mm^2. Representative high-magnification images were shown on the right. Scale bars represent 50 μm. All graphs represent means or individual values ± SEM. $^{**}P < 0.01$, $^{***}P < 0.001$ vs. LRP1$^{loxP/loxP}$ by two-sided Student's t-test.

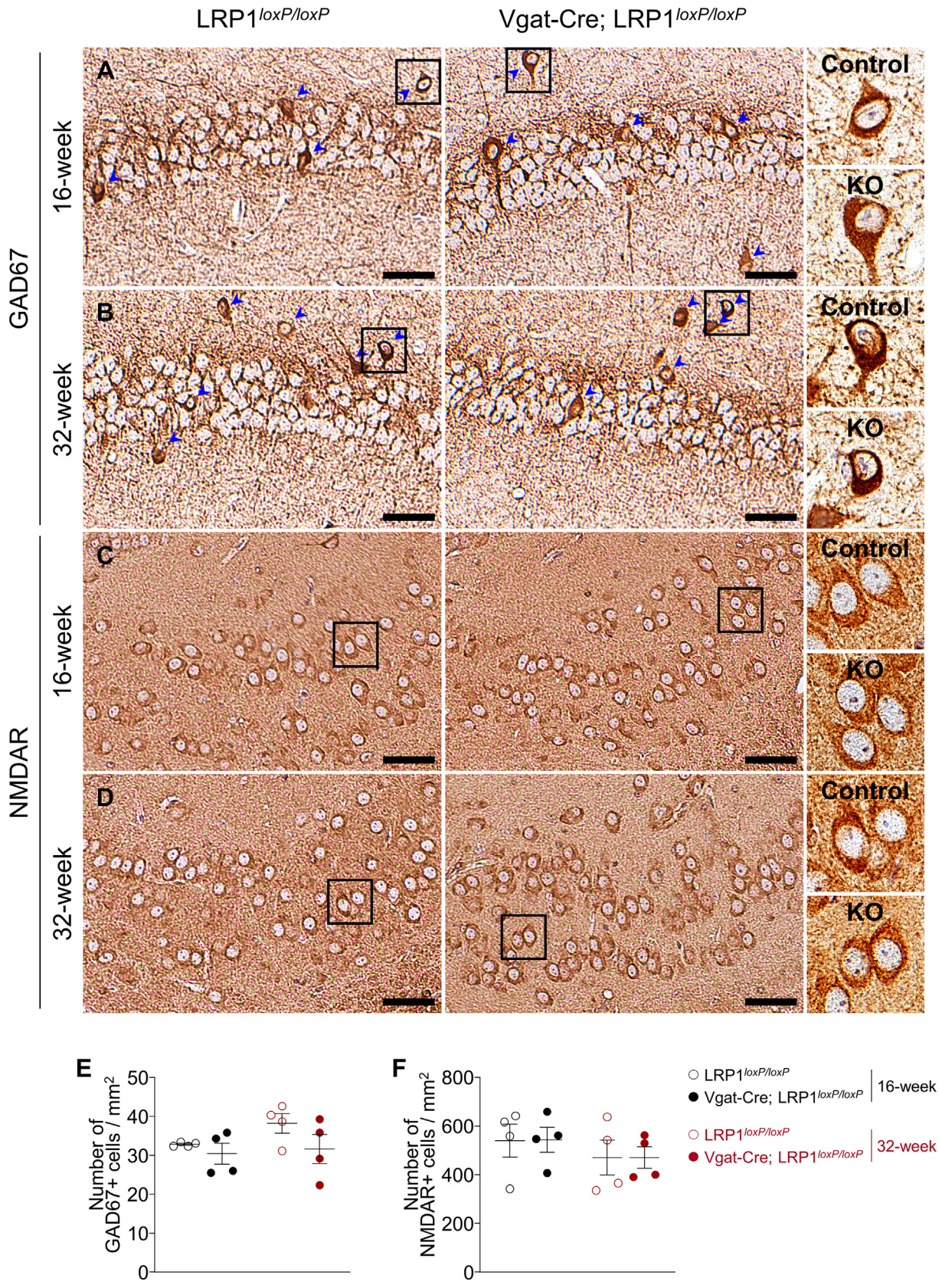

Figure 8: Immunohistochemical analysis of GAD67 and NMDAR in the hippocampus of GABAergic neuron-specific LRP1-deficient mice at different ages. (**A, B**) GAD67, and (**C, D**) NMDAR immunoreactivity of LRP1$^{loxP/loxP}$ and Vgat-Cre; LRP1$^{loxP/loxP}$ male mice at different ages (16 and 32 weeks old, n = 4 per group). Arrows indicate GAD67^{+} cells. GAD67^{+} cells and NMDAR^{+} cells were counted. Graphs represent the quantitation of GAD67^{+} and NMDAR^{+} cells in the whole hippocampal areas, which were normalized to mm^2. Scale bars represent 50 μm. All graphs show means ± SEM. $^{**}P < 0.01$, $^{***}P < 0.001$ vs. LRP1$^{loxP/loxP}$ by two-sided Student's t-test.

LRP1$^{loxP/loxP}$ mice but not in 16-week mice (Figure 6C). We also observed satellite microglial cells surrounding some neurons, known as perineuronal satellitosis, in the hippocampus of both LRP1$^{loxP/loxP}$ and Vgat-Cre; LRP1$^{loxP/loxP}$ mice. The number of these cells was markedly increased in the 32-week Vgat-Cre; LRP1$^{loxP/loxP}$ mice compared to the control group, but not in 16-week mice (Figure 6D). However, microglial cell proliferation remained unchanged in both 16-week and 32-week Vgat-Cre; LRP1$^{loxP/loxP}$ mice (Figure 6E). These results revealed that the increase in necrotic cells and satellitosis was caused by LRP1 deletion in GABAergic neurons of 32-week mice, while it did not impact the number of glial cells across the age of the mice (Figure 6C—E).

We further performed IHC for GFAP, IBA1, GAD67, and NMDAR in the hippocampus of Vgat-Cre; LRP1$^{loxP/loxP}$ mice. The number of immunoreactive GFAP^{+} and IBA1^{+} neurons in the hippocampus did not show any difference between LRP1$^{loxP/loxP}$ and Vgat-Cre; LRP1$^{loxP/loxP}$ mice, regardless of their age (Figure 7A—F). Similarly, LRP1 deletion didn't affect the number of the GAD67^{+} and NMDAR^{+} immunoreactive cells in 16-week and 32-week mice (Figure 8A—F). We found no difference in the gene expression of key molecules involved in inflammation between LRP1$^{loxP/loxP}$ and Vgat-Cre; LRP1$^{loxP/loxP}$ mice (Supplementary Figure 6A-E, G-L). We observed a reduction in the gene expression of NLRP3 in mice lacking LRP1 in GABAergic neurons (Supplementary Figure 6F). Moreover, we found that the levels of cleaved caspase-3 protein increased in the hippocampus of Vgat-Cre; LRP1$^{loxP/loxP}$ mice compared with LRP1$^{loxP/loxP}$ mice (Supplementary Figure 6M), suggesting that increased cleaved caspase-3 may promote apoptosis in Vgat-Cre; LRP1$^{loxP/loxP}$ mice, at least in part. Collectively, these findings demonstrate that LRP1 deletion from GABAergic neurons causes increased necrosis, satellitosis, and apoptosis, which may contribute to neurodegeneration and memory dysfunction. These neurodegenerative processes may be influenced by aging factors.

4. DISCUSSION

We showed that a deficiency in LRP1 in GABAergic neurons leads to obesity and metabolic disturbances, affecting reduced locomotor activity and impaired short- and long-term memory. The deletion of LRP1 can also negatively affect cognitive performance, as evidenced by the correlation between changes in obesity-related metabolic parameters and a decline in cognitive function caused by LRP1 deletion in GABAergic neurons. Pathological and IHC analysis demonstrate that LRP1 in GABAergic neurons plays a pivotal role in the progression of neuronal degeneration. Thus, LRP1 in GABAergic neurons is an important regulator of memory and cognitive function.

Our study revealed that when LRP1 is specifically deleted from GABAergic neurons, it can cause moderate impairment of motor coordination and locomotor activity. This is consistent with previous studies where LRP1 was generally deleted from the forebrain of mice, indicating the significant role of LRP1 in GABAergic neurons in motor function [36,37]. However, experimental evidence demonstrated that reduction in motor coordination is also accompanied by increased adiposity, increased circulating insulin and leptin levels, glucose intolerance [38,39], and crosstalk between leptin and insulin signaling [40—42]. Moreover, while GABAergic LRP1 deleted mice were hypoactive and obese, non-obese mice with pan-neuronal LRP1 deletion exhibited hyperactive characteristics [37]. Thus, it is likely that the deletion of GABAergic LRP1 causes neuronal dysfunction, which may contribute to the development of motor abnormalities and impaired energy balance.

Obesity has been linked to deficits in learning and memory [43,44]. One possible mechanism for this is that excess insulin leads to an increase in the cerebral inflammatory response and Aβ levels, which may contribute to the negative impact of obesity on working memory [45]. Supporting this, our memory behavior tests, such as the water T-maze and fear conditioning, along with correlation analysis, confirmed that obesity and its associated metabolic changes, including hyperinsulinemia, hyperleptinemia, and high levels of ApoJ, are associated with poor memory performance. Moreover, histopathological and immunohistochemical analyses showed that 32-week mice with a deficiency of LRP1 in their GABAergic neurons had increased satellite cells and neuronal death. These findings were not observed in 16-week mice with the LRP1 deficiency in GABAergic neurons, suggesting that the histopathological changes are age-dependent and may be affected by age-related risk factors such as obesity.

During the water T maze test, the significant effects of LRP1 deficiency on spatial memory and learning are only observed on day 1 but not on days 2—5. When we plotted 1—10 trials of day 1 for the acquisition water T maze and reversal water T maze tests (not shown), we found that both groups of mice initiated the task from similar starting points during acquisition. However, Vgat-Cre; LRP1$^{loxP/loxP}$ mice show a more erratic progression than LRP1$^{loxP/loxP}$ mice. This suggests that Vgat-Cre; LRP1$^{loxP/loxP}$ mice might require additional time to grasp the task on the first day. Several factors could contribute to this delay, including heightened side preference, increased stress response to water, or deficits in learning abilities specific to this mouse strain. The reversal test also revealed that Vgat-Cre; LRP1$^{loxP/loxP}$ mice display a slow learning ability on the first day. Therefore, we need further investigations to understand the underlying mechanisms for this slower learning ability in Vgat-Cre; LRP1$^{loxP/loxP}$ mice.

Of note, we cannot exclude the possibility that other neuronal populations, apart from the hippocampus, may also play a role in learning and memory processes in Vgat-Cre; LRP1$^{loxP/loxP}$ mice. Specifically, those that are functionally connected to the hippocampus may be involved. Furthermore, it is possible that only 10—15% of the GABAergic neurons in the hippocampus may be sufficient to regulate memory function in our experimental mice [46—48].

Transgenic mice with Alzheimer's disease fed sucrose-sweetened water developed glucose intolerance and hyperinsulinemia in the absence of obesity, which exacerbated memory impairment and increased insoluble Aβ protein deposition [49]. Additionally, leptin has been shown to facilitate spatial learning and memory performance, and leptin deficiency resulted in impaired spatial memory in rodents [50—52]. However, our LRP1-deficient mice with memory and learning deficits exhibited increased leptin levels. Given that GABAergic LRP1-deficient mice are obese but not leptin-resistant [14], it is conceivable that leptin may not be involved in learning and memory performance in our mice.

The fact that a lack of LRP1 in GABAergic neurons led to cognitive dysfunction may be associated with the neurodegeneration observed in the hippocampus. The majority (80—90%) of the hippocampal neurons are principal cells, while the minority are GABAergic neurons (10—15%) [46]. However, the inhibitory GABAergic neurons are highly integrated and show functionally diverse properties, allowing them to control the spatiotemporal functions of the rest of the hippocampus [47,48]. Thus, physiological and morphological changes in these neurons may affect overall hippocampal function. Here, we demonstrate that a deficiency of LRP1 in GABAergic neurons causes moderate-to-severe neurodegeneration, as evidenced by the increased number of cells with necrosis and satellitosis in the hippocampal area.

Morphophysiologically, excitatory principal cells of the hippocampus are pyramidal neurons located in specific areas such as the stratum pyramidale, while GABAergic interneurons are scattered throughout the hippocampus [53]. NMDAR-mediated excitatory glutamatergic neurotransmission critically regulates neuronal function, connectivity, and cell survival [54–57]. In the hippocampus, the cellular processes that control learning and memory are regulated by NMDAR [55,57]. However, we did not see any significant alteration in the number of inhibitory GAD67$^+$ cells or that of glutamatergic NMDAR$^+$ neurons, regardless of the age of the mice. Thus, the neurodegeneration in the hippocampus due to the deletion of LRP1 in GABAergic neurons may not directly result from the cellular death of either GAD67$^+$ or NMDAR$^+$ neurons. A yet-unidentified mechanism may be involved in this event.

The Extracellular matrix (ECM), surrounding GABAergic interneurons potentially influences synaptic changes. Particularly, Perineuronal nets (PNNs), a type of ECM localized at neuronal dendrites or synapses, play a crucial role in synaptic structure and function in the central nervous system (CNS) [58,59]. They envelop GABAergic interneurons, including those in the hippocampus, impacting synaptic plasticity and memory [58–61]. Suppression of PNNs may disrupt inhibitory circuit activity, affecting synapse physiology [62–64]. LRP1, found on the cell membrane, interacts with ECM molecules, modulating their composition and structure [65]. It is thus possible that deletion of LRP1 in GABAergic interneurons could contribute to synaptic and PNN alterations, disrupting the balance between excitatory and inhibitory circuits and potentially leading to learning and memory deficits. Further investigation is needed for a better understanding of this mechanism. The observation of increased necrosis and satellitosis, coupled with a lack of glial cell proliferation, raises questions about how LRP1 deficiency in GABAergic neurons causes these alterations. While satellitosis remains relatively underexplored, existing literature suggests its association with neuronal epilepsy [66]. Satellitosis involves the elimination of axonal terminals by satellite cells, favoring inhibitory axosomatic synapses and disrupting the balance between excitatory and inhibitory inputs, which could precipitate epileptic conditions [67]. Interestingly, this process of synaptic pruning is purportedly mediated by complement component C3 (C3) at the presynaptic terminal of GABAergic neurons, acting through CX3C chemokine receptor 1 (CX3CR1) on glial cells [68]. Notably, C3 is one of the ligands of LRP1, which also participates in the endocytosis of the active form of C3 [69]. This suggests a potential regulatory role of LRP1 expression on GABAergic neurons in the elimination of inhibitory synapses by glial cells, possibly as a protective mechanism against excitotoxicity or neuronal epilepsy. However, further investigation is warranted to determine whether LRP1 deficiency in GABAergic neurons heightens inhibitory synaptic pruning, exacerbating excitotoxicity and ultimately contributing to neurodegeneration.

5. CONCLUSIONS

LRP1 deletion in GABAergic neurons resulted in behavior abnormalities, cognitive deficits, and neurodegeneration, which may be age-dependent. Thus, LRP1 in GABAergic neurons may be an important regulator of memory and cognitive function.

CREDIT AUTHORSHIP CONTRIBUTION STATEMENT

Kellen Cristina da Cruz Rodrigues: Writing — original draft, Methodology, Investigation, Formal analysis, Conceptualization. **Seung Chan Kim:** Writing — original draft, Investigation, Formal analysis, Conceptualization. **Aaron Aykut Uner:** Writing — original draft, Investigation, Formal analysis, Conceptualization. **Zhi-Shuai Hou:** Methodology, Formal analysis, Conceptualization. **Jennie Young:** Formal analysis. **Clara Campolim:** Formal analysis. **Ahmet Aydogan:** Formal analysis. **Brendon Chung:** Formal analysis. **Anthony Choi:** Formal analysis. **Won-Mo Yang:** Formal analysis. **Woojin S. Kim:** Conceptualization. **Vincent Prevot:** Conceptualization. **Barbara J. Caldarone:** Formal analysis, Data curation. **Hyon Lee:** Writing — original draft, Conceptualization. **Young-Bum Kim:** Writing — review & editing, Writing — original draft, Investigation, Funding acquisition, Data curation, Conceptualization.

ACKNOWLEDGMENTS

This work was supported by grants from the National Institutes of Health (R01DK106076, R01DK123002, R01DK129946, R01AG080842 to YBK). K.C.R is a recipient of the fellowship from the São Paulo Research Foundation from Brazil (FAPESP 2019/19938-5), and A.A. is a recipient of the fellowship from the Scientific and Technological Research Council of Turkey (TUBITAK, 1059B192100216). We thank Brad Lowell for the Vgat-IRES-Cre recombinase mice and all members of the Kim lab for their helpful advice and discussions. We also thank Brad Hyman for his critical reading and Jongkyun Kang for his technical support on IHC experiments. We are grateful to the Histology Core at Beth Israel Deaconess Medical Center.

DECLARATION OF COMPETING INTEREST

The authors declare that they have no known competing financial interests or personal relationships that could have appeared to influence the work reported in this paper.

DATA AVAILABILITY

Data will be made available on request.

APPENDIX A. SUPPLEMENTARY DATA

Supplementary data to this article can be found online at https://doi.org/10.1016/j.molmet.2024.101941.

REFERENCES

[1] Anstey KJ, Cherbuin N, Budge M, Young J. Body mass index in midlife and late-life as a risk factor for dementia: a meta-analysis of prospective studies. Obes Rev: Off J Int Assoc Study Obesity 2011;12(5):e426–37. https://doi.org/10.1111/j.1467-789X.2010.00825.x.

[2] Fitzpatrick AL, Kuller LH, Lopez OL, Diehr P, O'Meara ES, Longstreth WT, et al. Midlife and late-life obesity and the risk of dementia: cardiovascular health study. Arch Neurol 2009;66(3):336–42. https://doi.org/10.1001/archneurol.2008.582.

[3] Jahn H. Memory loss in Alzheimer's disease. Dialogues Clin Neurosci 2013;15(4):445–54. https://doi.org/10.31887/DCNS.2013.15.4/hjahn.

[4] Lane CA, Hardy J, Schott JM. Alzheimer's disease. Eur J Neurol 2018;25(1):59–70. https://doi.org/10.1111/ene.13439.

[5] Profenno LA, Porsteinsson AP, Faraone SV. Meta-analysis of Alzheimer's disease risk with obesity, diabetes, and related disorders. Biol Psychiatr 2010;67(6):505–12. https://doi.org/10.1016/j.biopsych.2009.02.013.

[6] Serlin Y, Levy J, Shalev H. Vascular pathology and blood-brain barrier disruption in cognitive and psychiatric complications of type 2 diabetes

mellitus. Cardiovasc Psychiatry Neurol 2011;2011:609202. https://doi.org/10.1155/2011/609202.

[7] Cho S, Lee H, Seo J. Impact of genetic risk factors for Alzheimer's disease on brain glucose metabolism. Mol Neurobiol 2021;58(6):2608–19. https://doi.org/10.1007/s12035-021-02297-x.

[8] de Leon MJ, Convit A, Wolf OT, Tarshish CY, DeSanti S, Rusinek H, et al. Prediction of cognitive decline in normal elderly subjects with 2-[(18)F]fluoro-2-deoxy-D-glucose/poitron-emission tomography (FDG/PET). Proc Natl Acad Sci USA 2001;98(19):10966–71. https://doi.org/10.1073/pnas.191044198.

[9] Drzezga A, Lautenschlager N, Siebner H, Riemenschneider M, Willoch F, Minoshima S, et al. Cerebral metabolic changes accompanying conversion of mild cognitive impairment into Alzheimer's disease: a PET follow-up study. Eur J Nucl Med Mol Imag 2003;30(8):1104–13. https://doi.org/10.1007/s00259-003-1194-1.

[10] Gordon BA, Blazey TM, Su Y, Hari-Raj A, Dincer A, Flores S, et al. Spatial patterns of neuroimaging biomarker change in individuals from families with autosomal dominant Alzheimer's disease: a longitudinal study. Lancet Neurol 2018;17(3):241–50. https://doi.org/10.1016/S1474-4422(18)30028-0.

[11] Liu F, Shi J, Tanimukai H, Gu J, Gu J, Grundke-Iqbal I, et al. Reduced O-GlcNAcylation links lower brain glucose metabolism and tau pathology in Alzheimer's disease. Brain: J Neurol 2009;132(Pt 7):1820–32. https://doi.org/10.1093/brain/awp099.

[12] Moloney AM, Griffin RJ, Timmons S, O'Connor R, Ravid R, O'Neill C. Defects in IGF-1 receptor, insulin receptor and IRS-1/2 in Alzheimer's disease indicate possible resistance to IGF-1 and insulin signalling. Neurobiol Aging 2010;31(2):224–43. https://doi.org/10.1016/j.neurobiolaging.2008.04.002.

[13] Mosconi L, Tsui WH, Rusinek H, De Santi S, Li Y, Wang G-J, et al. Quantitation, regional vulnerability, and kinetic modeling of brain glucose metabolism in mild Alzheimer's disease. Eur J Nucl Med Mol Imag 2007;34(9):1467–79. https://doi.org/10.1007/s00259-007-0406-5.

[14] Kang M-C, Seo JA, Lee H, Uner A, Yang W-M, Cruz Rodrigues KC da, et al. LRP1 regulates food intake and energy balance in GABAergic neurons independently of leptin action. Am J Physiol Endocrinol Metab 2021;320(2):E379–89. https://doi.org/10.1152/ajpendo.00399.2020.

[15] Liu Q, Zhang J, Zerbinatti C, Zhan Y, Kolber BJ, Herz J, et al. Lipoprotein receptor LRP1 regulates leptin signaling and energy homeostasis in the adult central nervous system. PLoS Biol 2011;9(1):e1000575. https://doi.org/10.1371/journal.pbio.1000575.

[16] Fuentealba RA, Liu Q, Kanekiyo T, Zhang J, Bu G. Low density lipoprotein receptor-related protein 1 promotes anti-apoptotic signaling in neurons by activating Akt survival pathway. J Biol Chem 2009;284(49):34045–53. https://doi.org/10.1074/jbc.M109.021030.

[17] Bu G. Apolipoprotein E and its receptors in Alzheimer's disease: pathways, pathogenesis and therapy. Nat Rev Neurosci 2009;10(5):333–44. https://doi.org/10.1038/nrn2620.

[18] Lillis AP, Van Duyn LB, Murphy-Ullrich JE, Strickland DK. LDL receptor-related protein 1: unique tissue-specific functions revealed by selective gene knockout studies. Physiol Rev 2008;88(3):887–918. https://doi.org/10.1152/physrev.00033.2007.

[19] Shibata M, Yamada S, Kumar SR, Calero M, Bading J, Frangione B, et al. Clearance of Alzheimer's amyloid-ss(1-40) peptide from brain by LDL receptor-related protein-1 at the blood-brain barrier. J Clin Investig 2000;106(12):1489–99. https://doi.org/10.1172/JCI10498.

[20] Van Uden E, Mallory M, Veinbergs I, Alford M, Rockenstein E, Masliah E. Increased extracellular amyloid deposition and neurodegeneration in human amyloid precursor protein transgenic mice deficient in receptor-associated protein. J Neurosci: Off J Soc Neurosci 2002;22(21):9298–304. https://doi.org/10.1523/JNEUROSCI.22-21-09298.2002.

[21] Fuentealba RA, Liu Q, Zhang J, Kanekiyo T, Hu X, Lee J-M, et al. Low-density lipoprotein receptor-related protein 1 (LRP1) mediates neuronal Abeta42 uptake and lysosomal trafficking. PLoS One 2010;5(7):e11884. https://doi.org/10.1371/journal.pone.0011884.

[22] Kang DE, Pietrzik CU, Baum L, Chevallier N, Merriam DE, Kounnas MZ, et al. Modulation of amyloid beta-protein clearance and Alzheimer's disease susceptibility by the LDL receptor-related protein pathway. J Clin Investig 2000;106(9):1159–66. https://doi.org/10.1172/JCI11013.

[23] Storck SE, Meister S, Nahrath J, Meißner JN, Schubert N, Di Spiezio A, et al. Endothelial LRP1 transports amyloid-β(1-42) across the blood-brain barrier. J Clin Investig 2016;126(1):123–36. https://doi.org/10.1172/JCI81108.

[24] Knopp JL, Holder-Pearson L, Chase JG. Insulin units and conversion factors: a story of truth, boots, and faster half-truths. J Diabetes Sci Technol 2019;13(3):597–600. https://doi.org/10.1177/1932296818805074.

[25] Matthews DR, Hosker JP, Rudenski AS, Naylor BA, Treacher DF, Turner RC. Homeostasis model assessment: insulin resistance and beta-cell function from fasting plasma glucose and insulin concentrations in man. Diabetologia 1985;28(7):412–9. https://doi.org/10.1007/BF00280883.

[26] Luna LG. Manual of histologic staining methods of the armed forces Institute of pathology. 3rd ed. New York: McGraw-Hill; 1968. Blakiston Division.

[27] Charnay Y, Imhof A, Vallet PG, Kovari E, Bouras C, Giannakopoulos P. Clusterin in neurological disorders: molecular perspectives and clinical relevance. Brain Res Bull 2012;88(5):434–43. https://doi.org/10.1016/j.brainresbull.2012.05.006.

[28] Elias-Sonnenschein LS, Bertram L, Visser PJ. Relationship between genetic risk factors and markers for Alzheimer's disease pathology. Biomarkers Med 2012;6(4):477–95. https://doi.org/10.2217/bmm.12.56.

[29] Nuutinen T, Suuronen T, Kauppinen A, Salminen A. Clusterin: a forgotten player in Alzheimer's disease. Brain Res Rev 2009;61(2):89–104. https://doi.org/10.1016/j.brainresrev.2009.05.007.

[30] Yu J-T, Tan L. The role of clusterin in Alzheimer's disease: pathways, pathogenesis, and therapy. Mol Neurobiol 2012;45(2):314–26. https://doi.org/10.1007/s12035-012-8237-1.

[31] Hammad SM, Ranganathan S, Loukinova E, Twal WO, Argraves WS. Interaction of apolipoprotein J-amyloid beta-peptide complex with low density lipoprotein receptor-related protein-2/megalin. A mechanism to prevent pathological accumulation of amyloid beta-peptide. J Biol Chem 1997;272(30):18644–9. https://doi.org/10.1074/jbc.272.30.18644.

[32] Kounnas MZ, Moir RD, Rebeck GW, Bush AI, Argraves WS, Tanzi RE, et al. LDL receptor-related protein, a multifunctional ApoE receptor, binds secreted beta-amyloid precursor protein and mediates its degradation. Cell 1995;82(2):331–40. https://doi.org/10.1016/0092-8674(95)90320-8.

[33] Kwon MJ, Ju T-J, Heo J-Y, Kim Y-W, Kim J-Y, Won K-C, et al. Deficiency of clusterin exacerbates high-fat diet-induced insulin resistance in male mice. Endocrinology 2014;155(6):2089–101. https://doi.org/10.1210/en.2013-1870.

[34] Seo JA, Kang M-C, Ciaraldi TP, Kim SS, Park KS, Choe C, et al. Circulating ApoJ is closely associated with insulin resistance in human subjects. Metab, Clin Exp 2018;78:155–66. https://doi.org/10.1016/j.metabol.2017.09.014.

[35] Won JC, Park C-Y, Oh SW, Lee ES, Youn B-S, Kim M-S. Plasma clusterin (ApoJ) levels are associated with adiposity and systemic inflammation. PLoS One 2014;9(7):e103351. https://doi.org/10.1371/journal.pone.0103351.

[36] Liu Q, Trotter J, Zhang J, Peters MM, Cheng H, Bao J, et al. Neuronal LRP1 knockout in adult mice leads to impaired brain lipid metabolism and progressive, age-dependent synapse loss and neurodegeneration. J Neurosci: Off J Soc Neurosci 2010;30(50):17068–78. https://doi.org/10.1523/JNEUROSCI.4067-10.2010.

[37] May P, Rohlmann A, Bock HH, Zurhove K, Marth JD, Schomburg ED, et al. Neuronal LRP1 functionally associates with postsynaptic proteins and is required for normal motor function in mice. Mol Cell Biol 2004;24(20):8872–83. https://doi.org/10.1128/MCB.24.20.8872-8883.2004.

[38] Stojakovic A, A Mastronardi C, Licinio J, Wong M-L. Long-term consumption of high-fat diet impairs motor coordination without affecting the general motor activity. J Transl Sci 2019;5(5). https://doi.org/10.15761/JTS.1000295.

[39] Smith SM, Pjetri E, Friday WB, Presswood BH, Ricketts DK, Walter KR, et al. Aging-related behavioral, adiposity, and glucose impairments and their association following prenatal alcohol exposure in the C57BL/6J mouse. Nutrients 2022;14(7). https://doi.org/10.3390/nu14071438.

[40] Huo L, Gamber K, Greeley S, Silva J, Huntoon N, Leng X-H, et al. Leptin-dependent control of glucose balance and locomotor activity by POMC neurons. Cell Metabol 2009;9(6):537–47. https://doi.org/10.1016/j.cmet.2009.05.003.

[41] Sartorius T, Heni M, Tschritter O, Preissl H, Hopp S, Fritsche A, et al. Leptin affects insulin action in astrocytes and impairs insulin-mediated physical activity. Cell Physiol Biochem: Int J Experimental Cell Physiol Biochem Pharmacol 2012;30(1):238–46. https://doi.org/10.1159/000339060.

[42] Wang C, Chan JSY, Ren L, Yan JH. Obesity reduces cognitive and motor functions across the lifespan. Neural Plast 2016;2016:2473081. https://doi.org/10.1155/2016/2473081.

[43] Coppin G, Nolan-Poupart S, Jones-Gotman M, Small DM. Working memory and reward association learning impairments in obesity. Neuropsychologia 2014;65:146–55. https://doi.org/10.1016/j.neuropsychologia.2014.10.004.

[44] Gunstad J, Paul RH, Cohen RA, Tate DF, Gordon E. Obesity is associated with memory deficits in young and middle-aged adults. Eat Weight Disord : EWD 2006;11(1):e15–9. https://doi.org/10.1007/BF03327747.

[45] Craft S. Insulin resistance syndrome and Alzheimer's disease: age- and obesity-related effects on memory, amyloid, and inflammation. Neurobiol Aging 2005;26(Suppl 1):65–9. https://doi.org/10.1016/j.neurobiolaging.2005.08.021.

[46] Keller D, Erö C, Markram H. Cell densities in the mouse brain: a systematic review. Front Neuroanat 2018;12:83. https://doi.org/10.3389/fnana.2018.00083.

[47] Booker SA, Vida I. Morphological diversity and connectivity of hippocampal interneurons. Cell Tissue Res 2018;373(3):619–41. https://doi.org/10.1007/s00441-018-2882-2.

[48] Vida I, Degro CE, Booker SA. Morphology of hippocampal neurons. In: Cutsuridis V, Graham BP, Cobb S, Vida I, editors. Hippocampal microcircuits: a computational modeler's resource book. Cham: Springer International Publishing; 2018. p. 29–90.

[49] Cao D, Lu H, Lewis TL, Li L. Intake of sucrose-sweetened water induces insulin resistance and exacerbates memory deficits and amyloidosis in a transgenic mouse model of Alzheimer disease. J Biol Chem 2007;282(50):36275–82. https://doi.org/10.1074/jbc.M703561200.

[50] Li X-L, Aou S, Oomura Y, Hori N, Fukunaga K, Hori T. Impairment of long-term potentiation and spatial memory in leptin receptor-deficient rodents. Neuroscience 2002;113(3):607–15. https://doi.org/10.1016/s0306-4522(02)00162-8.

[51] Oomura Y, Aou S, Fukunaga K. Prandial increase of leptin in the brain activates spatial learning and memory. Pathophysiology: Off J Int Soc Pathophysiol 2010;17(2):119–27. https://doi.org/10.1016/j.pathophys.2009.04.004.

[52] Oomura Y, Hori N, Shiraishi T, Fukunaga K, Takeda H, Tsuji M, et al. Leptin facilitates learning and memory performance and enhances hippocampal CA1 long-term potentiation and CaMK II phosphorylation in rats. Peptides 2006;27(11):2738–49. https://doi.org/10.1016/j.peptides.2006.07.001.

[53] Pelkey KA, Chittajallu R, Craig MT, Tricoire L, Wester JC, McBain CJ. Hippocampal GABAergic inhibitory interneurons. Physiol Rev 2017;97(4):1619–747. https://doi.org/10.1152/physrev.00007.2017.

[54] Brigman JL, Wright T, Talani G, Prasad-Mulcare S, Jinde S, Seabold GK, et al. Loss of GluN2B-containing NMDA receptors in CA1 hippocampus and cortex impairs long-term depression, reduces dendritic spine density, and disrupts learning. J Neurosci: Off J Soc Neurosci 2010;30(13):4590–600. https://doi.org/10.1523/JNEUROSCI.0640-10.2010.

[55] Sakimura K, Kutsuwada T, Ito I, Manabe T, Takayama C, Kushiya E, et al. Reduced hippocampal LTP and spatial learning in mice lacking NMDA receptor epsilon 1 subunit. Nature 1995;373(6510):151–5. https://doi.org/10.1038/373151a0.

[56] Tolias KF, Bikoff JB, Burette A, Paradis S, Harrar D, Tavazoie S, et al. The Rac1-GEF Tiam1 couples the NMDA receptor to the activity-dependent development of dendritic arbors and spines. Neuron 2005;45(4):525–38. https://doi.org/10.1016/j.neuron.2005.01.024.

[57] Wong ROL, Ghosh A. Activity-dependent regulation of dendritic growth and patterning. Nat Rev Neurosci 2002;3(10):803–12. https://doi.org/10.1038/nrn941.

[58] Kosaka T, Heizmann CW. Selective staining of a population of parvalbumin-containing GABAergic neurons in the rat cerebral cortex by lectins with specific affinity for terminal N-acetylgalactosamine. Brain Res 1989;483(1):158–63. https://doi.org/10.1016/0006-8993(89)90048-6.

[59] Celio MR. Perineuronal nets of extracellular matrix around parvalbumin-containing neurons of the hippocampus. Hippocampus 1993;3(1 S):55–60.

[60] Carulli D, Verhaagen J. An extracellular perspective on CNS maturation: perineuronal nets and the control of plasticity. Int J Mol Sci 2021;22(5):1–26. https://doi.org/10.3390/ijms22052434.

[61] Fawcett JW, Fyhn M, Jendelova P, Kwok JCF, Ruzicka J, Sorg BA. The extracellular matrix and perineuronal nets in memory. Mol Psychiatr 2022;27(8):3192–203. https://doi.org/10.1038/s41380-022-01634-3.

[62] Gottschling C, Wegrzyn D, Denecke B, Faissner A. Elimination of the four extracellular matrix molecules tenascin-C, tenascin-R, brevican and neurocan alters the ratio of excitatory and inhibitory synapses. Sci Rep 2019;9(1):13939. https://doi.org/10.1038/s41598-019-50404-9.

[63] Romberg C, Yang S, Melani R, Andrews MR, Horner AE, Spillantini MG, et al. Depletion of perineuronal nets enhances recognition memory and long-term depression in the perirhinal cortex. J Neurosci: Off J Soc Neurosci 2013;33(16):7057–65. https://doi.org/10.1523/JNEUROSCI.6267-11.2013.

[64] Wingert JC, Sorg BA. Impact of perineuronal nets on electrophysiology of parvalbumin interneurons, principal neurons, and brain oscillations: a review. Front Synaptic Neurosci 2021;13:673210. https://doi.org/10.3389/fnsyn.2021.673210.

[65] Bres EE, Faissner A. Low density receptor-related protein 1 interactions with the extracellular matrix: more than meets the eye. Front Cell Dev Biol 2019;7(MAR):31. https://doi.org/10.3389/fcell.2019.00031.

[66] Sarnat HB, Flores-Sarnat L. Neuropathology of pediatric epilepsy. Handb Clin Neurol 2013;111:399–416. https://doi.org/10.1016/B978-0-444-52891-9.00044-0.

[67] Hirano A. Edema and myelin-associated extracellular spaces. Brain edema. Berlin, Heidelberg: Springer Berlin Heidelberg; 1985. p. 6–13.

[68] Schafer DP, Lehrman EK, Kautzman AG, Koyama R, Mardinly AR, Yamasaki R, et al. Microglia sculpt postnatal neural circuits in an activity and complement-dependent manner. Neuron 2012;74(4):691–705. https://doi.org/10.1016/j.neuron.2012.03.026.

[69] Meilinger M, Gschwentner C, Burger I, Haumer M, Wahrmann M, Szollar L, et al. Metabolism of activated complement component C3 is mediated by the low density lipoprotein receptor-related protein/alpha(2)-macroglobulin receptor. J Biol Chem 1999;274(53):38091–6. https://doi.org/10.1074/jbc.274.53.38091.

